International Journal of Multiphase Flow 125 (2020) 103195

Contents lists available at ScienceDirect

International Journal of Multiphase Flow

journal homepage: www.elsevier.com/locate/ijmulflow

Effect of computational domain size on inertial particle one-point statistics in open channel flow

Guiquan Wang[a,c,*], Hyungwon John Park[b], David H. Richter[a]

[a] Department of Civil and Environmental Engineering and Earth Sciences, University of Notre Dame, Notre Dame, IN 46556, USA
[b] Department of Aerospace and Mechanical Engineering, University of Notre Dame, Notre Dame, IN 46556, USA
[c] Physics of Fluids Group and Twente Max Planck Center, Department of Science and Technology, Mesa+ Institute, and J.M. Burgers Center for Fluid Dynamics, University of Twente, P.O Box 217 AE, Enschede 7500, the Netherlands

ARTICLE INFO

Article history:
Received 17 September 2019
Revised 13 December 2019
Accepted 27 December 2019
Available online 09 January 2020

Keywords:
Inertial particles
Wall turbulence
Simulations
Domain size
One-point statistics

ABSTRACT

Effects of the computational domain size on inertial particle one-point statistics are presented for direct numerical simulations of turbulent open channel flow at a moderate Reynolds number, which are seeded with two-way coupled particles at low volume concentration (less than 1.5×10^{-3}, for such particle load the one-way coupled particles scheme is also valid). Particle one-point statistics across a wide range of Stokes numbers for a small domain (which captures only one or two large-scale motions (LSMs) in the inner layer) and a medium domain (which captures only one or two very large-scale motions (VLSMs) in the outer layer), are compared with those from a reference large domain. Although in single-phase flow the medium domain size simulation reproduces the same fluid one-point statistics as those in a large domain size, in particle-laden flow, comparisons show certain discrepancies in the particle one-point statistics, such as particle accumulation close to the wall ($y^+ < 10$), maximum values of particle mean-squared streamwise velocity fluctuation, and particle Reynolds shear stress in the inner layer. The difference is larger for moderate Stokes numbers ($St^+ = 24.2$ and 60.5) compared to low ($St^+ = 2.42$) and very high ($St^+ = 908$) Stokes numbers, which is also enhanced by using a small domain size.

1. Introduction

Direct numerical simulation (DNS) of particle-laden open channel flow is used as a representative framework for an investigation of particle interaction with turbulent structures in environmental boundary layers (Pedinotti et al., 1992; Narayanan et al., 2003; Lovecchio et al., 2013; Richter and Chamecki, 2017; Wang and Richter, 2019b). As is done for most DNS of wall-bounded turbulence, doubly periodic boundary conditions are applied in two homogeneous (wall parallel) directions, however this artificial constraint results in inappropriate long-range correlations of large-scale turbulent structures (i.e. effectively infinite due to periodicity). With this in mind, it has remained an ongoing question on how large the domain size must be in order to accurately capture the largest flow scales and their corresponding statistics even in the simplest wall-bounded turbulence at moderate to high Reynolds number (Lozano-Durán and Jiménez, 2014).

Away from the region influenced directly by the surface, the energy spectra of turbulent structures and fluid one-point statistics in open channel flows are nearly identical with those in wall-bounded channel flows (Nakagawa and Nezu, 1981; Yamamoto et al., 2001; Nagaosa and Handler, 2003; Lovecchio et al., 2013; Wang and Richter, 2019b; 2019a). In wall-bounded turbulence, it is known that there are two distinct energetic structures, referred to as large-scale motions (LSMs) in the inner layer (Kline et al., 1967; Jiménez, 2011) and very-large-scale motions (VLSMs) in the outer layer (Del Álamo and Jiménez, 2003; Hutchins and Marusic, 2007). In the sense of providing accurate one-point statistics of unladen turbulent flow in the inner or the outer layers, existing work has been dedicated to determining the appropriate minimal domain size which is sufficiently large to capture LSMs or VLSMs. In the inner layer, by using a minimal flow unit (~ 100 wall units in spanwise), Hamilton et al. (1995) finds that there still exists a regeneration cycle process of the LSMs. Jiménez and Moin (1991) show that the low-order statistics are in good agreement with those of natural turbulence below $y^+ = 40$. Meanwhile, it is generally accepted that the regeneration cycle of LSMs in the inner layer is independent from VLSMs in the outer layer (Jiménez and Pinelli, 1999; Guala et al., 2006), although VLSMs can certainly

* Corresponding author at: Department of Civil and Environmental Engineering and Earth Sciences, University of Notre Dame, Notre Dame, IN 46556, USA.
E-mail addresses: g.wang@utwente.nl, gwang4academy@gmail.com (G. Wang), David.Richter.26@nd.edu (D.H. Richter).

https://doi.org/10.1016/j.ijmultiphaseflow.2019.103195
0301-9322/

Table 1
Domain size used by previous studies.

Ref.	*Domain size*	Re_τ	St^+
	Open channel flow		
Narayanan et al. (2003)	$2\pi h \times h \times \pi h$	$Re_\tau = 171$	5,15
Kidanemariam et al. (2013)	$12h \times h \times 3h$	$Re_\tau = 184$	4.9
Pan and Banerjee (1996)	$\pi h \times h \times \pi/2h$	$Re_\tau = 300$	< 1
Richter and Chamecki (2017)	$2\pi h \times h \times 2\pi h$	$Re_\tau = 315$	$0.9 - 46.5$
Lovecchio et al. (2013)	$2\pi h \times h \times \pi h$	$Re_\tau = 171, 509$	$0.06 - 1.0$
Wang and Richter (2019b)	$6\pi h \times h \times 2\pi h$	$Re_\tau = 550$	$2.42 - 908$
–	$10.8h \times h \times \pi h$	$Re_\tau = 950$	180.5,361
	Wall − bounded channel flow		
Marchioli et al. (2008)	$4\pi h \times 2h \times 2\pi h$	$Re_\tau = 150$	1,5,25
Sardina et al. (2012)	$4\pi h \times 2h \times 4/3\pi h$	$Re_\tau = 180$	$0 - 100$
–	$12\pi h \times 2h \times 4\pi h$	–	$0 - 100$
Zhao et al. (2013)	$12h \times 2h \times 6h$	$Re_\tau = 180$	5,30,50
Lee and Lee (2019)	$4\pi h \times 2h \times 2\pi h$	$Re_\tau = 180$	$1 - 20$
Wang et al. (2019)	$6\pi h \times 2h \times \pi h$	$Re_\tau = 227$	58.6
Capecelatro et al. (2018)	$20h \times 2h \times 3h$	$Re_\tau = 300$	63,630
Capecelatro and Desjardins (2015)	$4\pi h \times 2h \times 4/3\pi h$	$Re_\tau = 630$	90
Vreman (2015)	$6h \times 2h \times 2h$	$Re_\tau = 642$	2060

interact with LSMs (Kim and Adrian, 1999; Adrian and Marusic, 2012). In the outer layer, Hwang and Cossu (2010) demonstrate that VLSMs can be sustained only if the streamwise and spanwise domain sizes are larger than certain threshold values, i.e. $L_x \approx 3h$ and $L_z \approx 1.5h$, where h is the half-height of channel. However, in order to get correct low-order statistics in the logarithmic and outer regions, Flores and Jiménez (2010) and Lozano-Durán and Jiménez (2014) extended the minimal dimensions to be of the order of $L_x \approx 6h$ and $L_z \approx 3h$ in the streamwise and spanwise directions.

In particle-laden flow, obtaining the correct inertial particle one-point statistics is of great importance for developing new subgrid models (Vance et al., 2006) and Eulerian descriptions (Simonin et al., 1993) of the particle equations of motion. However in numerical simulations, choosing suitable computational domains in order to obtain particle one-point statistics which are independent of domain size is complicated by particle-turbulence interactions. Based on Sardina et al. (2012), the domain truncation effect (comparing a small domain size $4\pi h \times 2h \times 4/3\pi h$ with a large domain size $12\pi h \times 2h \times 4\pi h$) has a significant impact on particle distribution at a relatively low Reynolds number ($Re_\tau = 180$, $Re_\tau \equiv u_\tau h/\nu$, where h is the depth of the open channel). A surprising increase (up to 20%) of particle concentration near walls is found in the large domain with respect to the small domain, which is due to insufficient domain dimensions necessary to induce an artificial correlation in the velocity field, leading to a blocking of the effects of the particle aggregation. At a higher Reynolds number ($Re_\tau = 550$) with stronger influence from VLSMs than at low Reynolds number ($Re_\tau = 180$), similar results are also reported by Wang and Richter (2019a). Unfortunately, even though the domain size plays a crucial role in determining the particle one-point statistics, guidance of choosing the domain size is lacking in this regard.

Computational domain sizes used in selected published works are summarised and listed in Table 1. St^+ is a dimensionless particle Stokes relaxation time scale ($\tau_p \equiv \rho_p d_p^2/(18\rho_f \nu)$) normalized by the viscous time scale (ν/u_τ^2) (these terms to be defined in the next section). In an open channel flow configuration with increasing Reynolds number, Narayanan et al. (2003) studied particle deposition at $Re_\tau = 171$. Pan and Banerjee (1996) compared one-point statistics between simulations and experimental data at $Re_\tau = 300$. Richter and Chamecki (2017) investigated the role of particle inertia on modifying concentration profiles and vertical fluxes in the lowest few meters of the atmosphere at $Re_\tau = 315$. At higher Reynolds numbers, Lovecchio et al. (2013) studied the dispersion of light particles floating at $Re_\tau = 171$ and 509. Wang and Richter (2019b) discussed two modulation mechanisms of VLSMs by inertial particles at $Re_\tau = 550$ and 950. In wall-bounded channel flow, Marchioli et al. (2008) benchmarked low-order statistics of both particles and carrier phase at $Re_\tau = 150$. Zhao et al. (2013) studied the transfer of mechanical energy between particles and carrier phase at $Re_\tau = 180$. Lee and Lee (2019) considered the effect of wall-normal gravity on particle-laden flow near a wall at $Re_\tau = 180$. Wang et al. (2019) compared low- and high-order statistics and particle distributions at $Re_\tau = 227$ between numerical simulations and the experiments performed by Fong et al. (2019). Capecelatro et al. (2018) and Capecelatro and Desjardins (2015) explored turbulence transition at $Re_\tau = 300$ and the effects of particle clustering on the carrier-phase turbulence at $Re_\tau = 630$. Generally, in both open channel flow and wall-bounded channel flow configurations, previous work focuses on near-wall particle one-point statistics, particle preferential concentration, and particle clustering behaviour at a relatively low Reynolds numbers ($Re_\tau \approx 180$; those dominated by LSMs in the inner layer) (Pan and Banerjee, 1996; Narayanan et al., 2003; Marchioli et al., 2008; Zhao et al., 2013; Kidanemariam et al., 2013; Lee and Lee, 2019). Starting at low to moderate Reynolds numbers ($300 < Re_\tau < 642$) (Lovecchio et al., 2013; Capecelatro and Desjardins, 2015; Vreman, 2015; Richter and Chamecki, 2017; Capecelatro et al., 2018; Wang et al., 2019), due to the emergence of VLSMs in the outer layer, the domain size must be sufficiently large in both the streamwise and spanwise directions to statistically capture the VLSMs. This is necessary in order to reproduce identical particle/fluid one-point statistics as those in larger domain sizes. At the same time, imposing large simulation domains and large particle numbers is computationally expensive; it is therefore a present goal to determine a domain size which is large enough to include the influence of the VLSMs from the outer layer, but also small enough to reasonably obtain accurate particle one-point statistics in particle-laden turbulence at moderate to high Reynolds number.

As noted above, Lozano-Durán and Jiménez (2014) has examined the effect of domain size on fluid one-point statistics in single-phase, wall-bounded turbulence, finding that an intermediate domain size of $L_x \approx 6h$ and $L_z \approx 3h$ in outer scale reproduces nearly same fluid one-point statistics in the larger domains across the full channel height at moderate to high Reynolds numbers

($547 < Re_\tau < 4179$). After verifying results with Lozano-Durán and Jiménez (2014), we perform a similar analysis in order to investigate the effects of domain size on particle one-point statistics, particularly as it is influenced by the particle Stokes number (we consider $2.42 \leq St^+ \leq 908$). Since large particle inertia is associated with higher temporal and spatial correlation of velocity statistics, our goal is to characterize the necessary domain size which can reproduce accurate particle one-point statistics compared to larger domains.

2. Numerical setup

Direct numerical simulations of the carrier phase are performed for an incompressible Newtonian fluid. A pseudospectral method is employed in the periodic directions (streamwise x and spanwise z), and second-order finite differences are used for spatial discretization in wall-normal, y direction. The solution is advanced in time by a third-order Runge–Kutta scheme. Incompressibility is achieved via the solution of a pressure Poisson equation. The fluid velocity and pressure fields are a solution of the continuity and momentum balance equations in Eqs. (1) and (2), respectively:

$$\frac{\partial u_j}{\partial x_j} = 0, \tag{1}$$

$$\frac{\partial u_i}{\partial t} + u_j \frac{\partial u_i}{\partial x_j} = -\frac{1}{\rho_f}\frac{\partial p}{\partial x_i} + \nu \frac{\partial^2 u_i}{\partial x_j \partial x_j} + \frac{1}{\rho_f} F_i. \tag{2}$$

Here u_i is the fluid velocity, p is the pressure, F_i is the particle feedback force to the carrier phase computed by summing and projecting the particle force to the nearest Eulerian grid points, ν is the fluid kinematic viscosity, and ρ_f is the fluid density.

Particle trajectories and particle-laden flow dynamics are based on the point-force approximation where the particle-to-fluid density ratio $r \equiv \rho_p/\rho_f \gg 1$ and the particle size is smaller than the smallest viscous dissipation scales of the turbulence. As a consequence of this and the low volume concentrations (a maximum bulk volume fraction of $\overline{\Phi_V}$ less than 1×10^{-3}), only the Schiller-Naumann (Schiller, 1933) hydrodynamic drag force is considered. The velocity of particle n is governed by Eq. (3) and particle trajectories are then obtained from numerical integration of the equation of motion in Eq. (4):

$$\frac{du_{p,i}^n}{dt} = f_i^n, \tag{3}$$

$$\frac{dx_i^n}{dt} = u_{p,i}^n, \tag{4}$$

where the drag is given by

$$f_i^n = \frac{1}{\tau_p}\left[1 + 0.15(Re_p^n)^{0.687}\right]\left(u_{f,i}^n - u_{p,i}^n\right). \tag{5}$$

Here, $\tau_p = \rho_p {d_p}^2/18\mu$ is the Stokes relaxation time of the particle, and the particle Reynolds number $Re_p^n = \mid u_{f,i}^n - u_{p,i}^n \mid d_p^n/\nu$ is based on the magnitude of the particle slip velocity $(u_{f,i}^n - u_{p,i}^n)$ and particle diameter d_p^n. In this work, the average Re_p^n is less than 1.0, which is far smaller than the suggested maximum $Re_p \approx 800$ for the Stokes drag correction in Eq. (5). As a result of the low Re_p, the correction to the Stokes drag is minimal in this study. Other terms in the particle momentum equation (Maxey and Riley, 1983) are neglected since they remain small compared with drag when the density ratio $r \gg 1$. In all simulations, particles are initially distributed at random locations throughout the channel. Particle-particle collisions are not taken into consideration, and we exert a purely elastic collision between particles and the lower wall and the free-surface of the open channel flow. Gravity is not included so as to focus specifically on the role of turbulence in particle transport. For validation of the implementation of this model, comparisons against the code of Capecelatro and Desjardins (2013) are performed for inertial particles of $St^+ = 30 - 2000$. We also compare this code with published numerical and experimental results; details can be found in Wang et al. (2019).

The fluid-phase flow parameters are provided in Table 2. Throughout, the subscripts "S", "M" and "L" refer to large, medium and small domain sizes, which are simulated for both unladen flow and particle-laden flow. The doubled size of the large domain in the streamwise direction (subscript "DL") is only used in single-phase flow simulation to test if the large domain size is sufficiently large to capture domain-independent fluid one-point statistics across the full channel height. The friction Reynolds number is defined as $Re_\tau \equiv u_\tau h/\nu$, where h is the depth of the open channel. The superscript "+" refers to quantities normalized by the viscous scales, where δ_ν, u_τ and ν/u_τ^2 correspond to the viscous length scale, velocity scale, and time scale, respectively.

The relevant particle parameters are listed in Table 3. d_p is the particle diameter, which is maintained as a constant for the different Stokes numbers. The ratio d_p/η_K is maintained at a value of approximately 0.42, where η_K is the vertically averaged Kolmogorov length scale. Φ_m is the particle mass concentration and N_p is the total particle number. We choose the same $\Phi_m = 0.14$ for $case3-6$ whereas a low mass loading $\Phi_m = 0.024$ is used in $case2$. Particle Stokes numbers based on the inner viscous time scale correspond to $St^+ = 2.42 - 908$ for $case2-6$.

3. One-point statistics of unladen flow

Contours of instantaneous streamwise velocity fluctuation (u') at two x-z planes ($y^+ = 55$ and $y^+ = 275$) in unladen flow are shown in Fig. 1, and illustrate the ubiquitous streaky structures in the inner and outer layers. Panels(a–d) refer to decreasing domain sizes: (a) doubled L_x of the large domain ($case1_{DL}$), (b) large domain ($case1_L$), (c) medium domain ($case1_M$), (d) and small domain ($case1_S$) as listed in Table 2. In both the inner and outer layers, strong and alternating positive and negative u' structures are visible in the spanwise direction, except in the outer layer of the small domain, i.e. the right panel of $case1_S$ in Fig. 1(d). In the inner layer, $case1_S$ with the small domain size only contains one or two near-wall coherent structures (LSMs). In spite of this, the regeneration cycle of the LSMs can be sustained in $case1_S$ whereas VLSMs in the outer layer cannot be captured by such a small domain size (Jiménez and Moin, 1991; Hamilton et al., 1995). With increasing of the domain size (Fig. 1(c)), $case1_M$ is sufficiently large to capture the LSMs in the inner layer in both the spanwise and streamwise directions (in the left panel), whereas this domain size only contains one or two VLSMs in outer scale (in the right panel). Continuing to increase the domain size, as shown in the right panel of Fig. 1(b), alternating streaky structures can be seen in the outer layer in both the spanwise and streamwise directions, which is qualitatively similar to the even larger domain size simulation, $case1_{DL}$, as shown in the bottom panel of Fig. 1(a). In general, these contour figures qualitatively indicate that (*i*) $case1_L$ can capture multiple LSMs and VLSMs with similar characteristics as those are in $case1_{DL}$, and can therefore be used as a reference domain size in particle-laden flow; and (*ii*) even though the domain size used in $case1_S$ and $case1_M$ only captures a limited number of confined structures in the inner and outer layers, the fluid one-point statistics of $case1_M$ agree very well with those in the larger domains $case1_L$ and $case1_{DL}$. This will be discussed and illustrated below in Fig. 2.

The fluid one-point statistics of four different domain sizes in open channel flow are compared with the published results of a very large domain size ($60\pi h \times 2h \times 6\pi h$) from Lozano-Durán and Jiménez (2014) in wall-bounded channel flow,

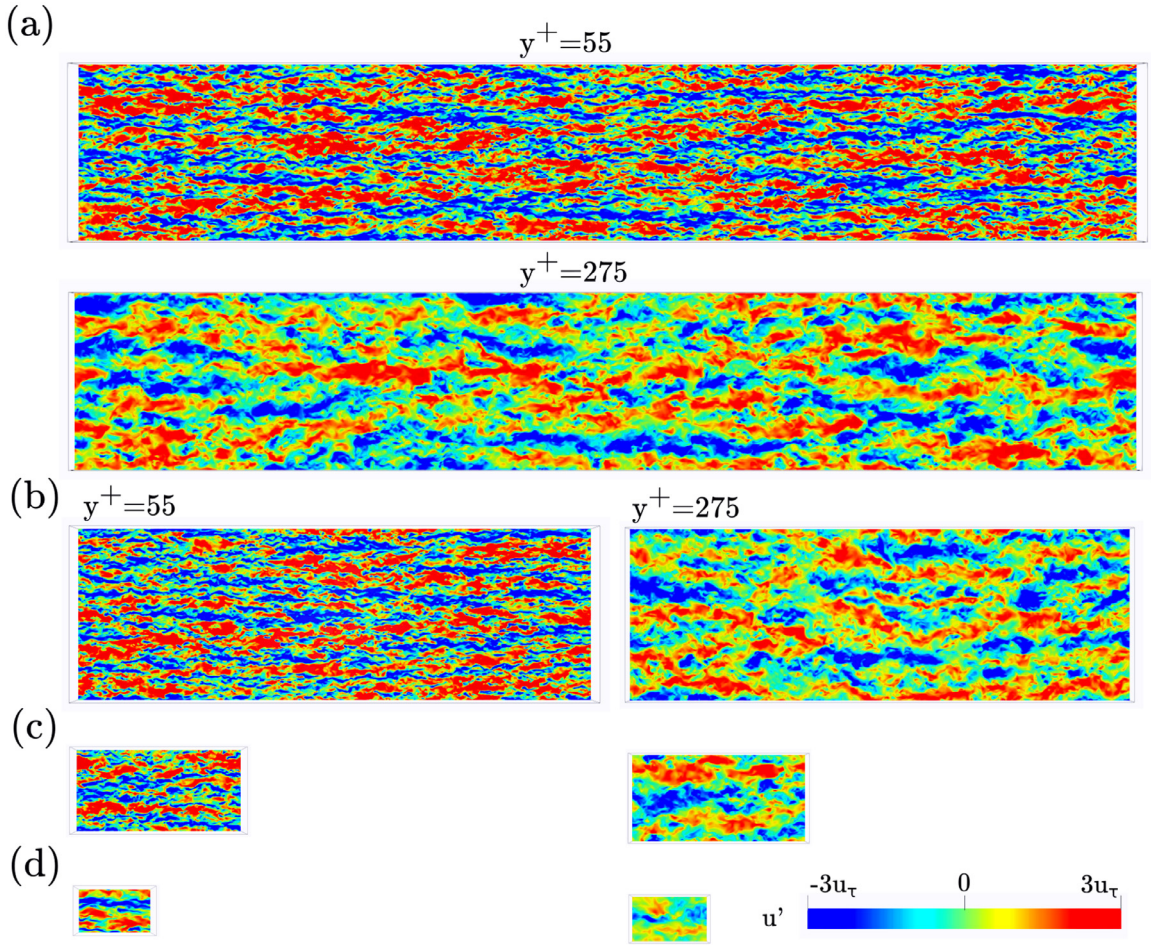

Fig. 1. (a) Contours of instantaneous streamwise velocity fluctuation u' at two xâz planes ($y^+ = 55$ and $y^+ = 275$) representing the inner and outer layers. Panels (a-d) refer to single-phase flow with four decreasing domain sizes $cases1_{DL,L,M,S}$ as listed in Table 2, respectively.

Table 2
Fluid phase parameters for DNS.

	Large(*L*)	*Medium*(*M*)	*Small*(*S*)	*Double x of large*(*DL*)
$Re_\tau = 550$				
N_x, N_y, N_z	1024,128,512	256,128,256	128,128,128	2048,128,512
L_x, L_y, L_z	6π, 1, 2π	6,1,3	2.5,1,1.5	12π, 1, 2π
L_x^+, L_y^+, L_z^+	10367,550,3456	3300,550,1650	1375,550,825	20734,550,3456
$\Delta_x^+, \Delta_y^+(wall, surface), \Delta_z^+$	10.1,(1,7.2),6.75	12.9,(1,7.2),6.45	10.7,(1,7.2),6.45	10.1,(1,7.2),6.75
$Re_\tau = 950$				
N_x, N_y, N_z	1024,256,512	512,256,512	256,256,256	–
L_x, L_y, L_z	3.5π, 1, π	6,1,3	2.5,1,1.5	–
L_x^+, L_y^+, L_z^+	10439,950,2985	5700,950,2850	2375,950,1425	–
$\Delta_x^+, \Delta_y^+(wall, surface), \Delta_z^+$	10.1,(1,6.4),5.83	11.13,(1,6.4),5.57	9.28,(1,6.4),5.57	–

Table 3
Particle parameters.

	case	Φ_m	ρ_p/ρ_f	Φ_V ($\times 10^{-4}$)	N_p(L,M,S) ($\times 10^6$)	τ_p	St^+
$Re_\tau = 550$	1_{L,M,S,DL}	Single-phase flow					
	2_{L,M,S}	0.024	16	15	12.6, 1.91, 0.398	0.51	2.42
	3_{L,M,S}	0.14	160	8.75	7.33, 1.11, 0.232	5.1	24.2
	4_{L,M,S}	0.14	400	3.5	2.93, 0.446, 0.0928	12.7	60.5
	5_{L,M,S}	0.14	1200	1.17	0.98, 0.15, 0.03	38.2	182
	6_{L,M,S}	0.14	6000	0.23	0.195, 0.03, 0.0062	191	908
$Re_\tau = 950$	7_{L,M,S}	0.14	350	4.0	1.68,0.89,0.186	2.78	39.8
	8_{L,M,S}	0.14	1600	0.875	0.37,0.19,0.04	12.7	182

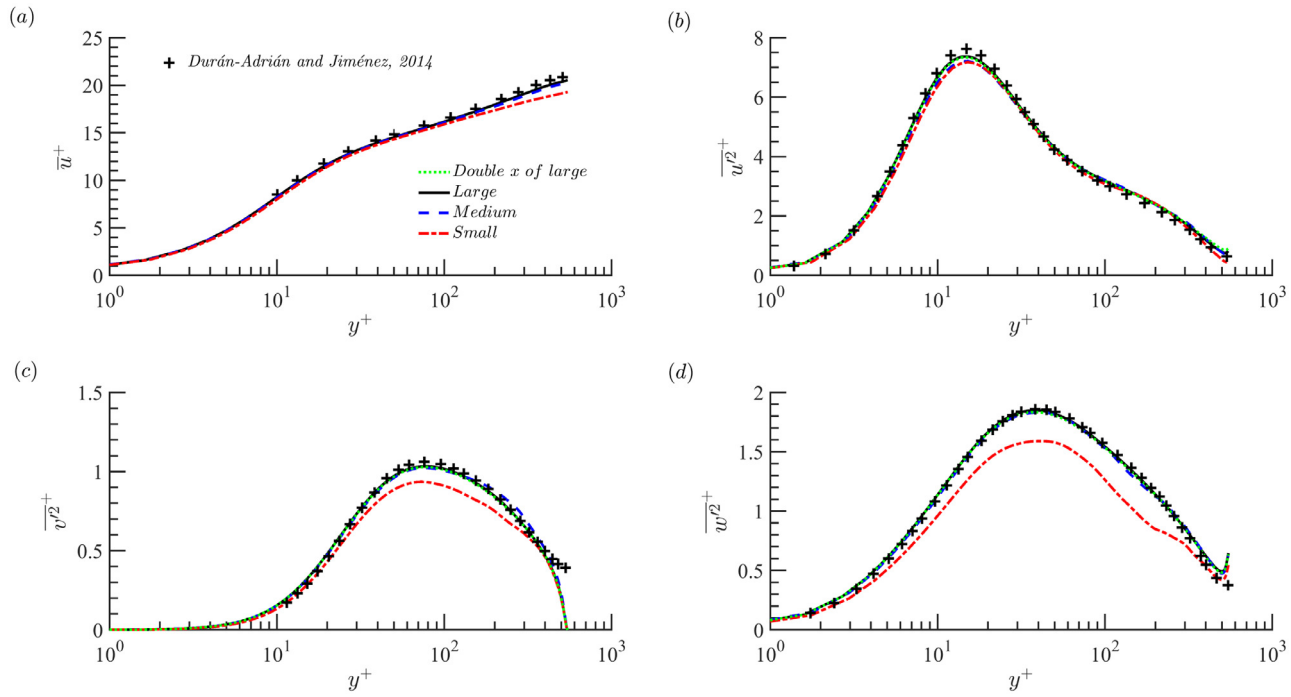

Fig. 2. Comparison of one-point statistics of unladen open-channel flow between four different domain sizes ($cases1_{DL,L,M,S}$) and published data from Lozano-Durán and Jiménez (2014) in a very large domain size ($60\pi h \times 2h \times 6\pi h$) in wall-bounded channel flow. (a) Mean streamwise velocity profile. (b–d) Streamwise, wall-normal, and spanwise mean-squared velocity fluctuations.

as shown in Fig. 2. In their work, the very large domain size at $Re_\tau = 550$ from Lozano-Durán and Jiménez (2014) is shown to be sufficiently large to capture domain-size-independent fluid one-point statistics, by comparing with other published studies (i.e., Moser et al. (1999) ($2\pi h \times 2h \times \pi h$ at $Re_\tau = 590$) and Del Álamo and Jiménez (2003) ($8\pi h \times 2h \times 4\pi h$ at $Re_\tau = 550$)). The fluid one-point statistics (mean streamwise velocity and mean-squared velocity fluctuations in three directions) agree very well between Del Álamo and Jiménez (2003) and Lozano-Durán and Jiménez (2014), whereas the smaller domain size used by Moser et al. (1999) is not large enough to achieve domain independent one-point statistics (not shown here).

Presently, the fluid one-point statistics of $cases1_{DL,L,M,S}$ are compared with the very large domain size simulation of Lozano-Durán and Jiménez (2014). The mean velocity and mean-squared velocity fluctuations in three directions can be found in Fig. 2(a–d), respectively. The one-point statistics of $case1_L$ are identical with those of $case1_{DL}$, and both agree well with the published data of Lozano-Durán and Jiménez (2014). For the small domain size, comparing between $case1_S$ and $case1_L$, the mean velocity profiles almost overlap in the inner layer ($y^+ < 100$) whereas a discrepancy emerges in the outer layer, especially for $y^+ > 200$. The streamwise mean-squared velocity fluctuation is similar between the domain sizes, except that the peak ($10 < y^+ < 20$) of $\overline{u'^2}^+$ is slightly smaller ($< 3\%$) in the small domain compared to the large domain. A more remarkable difference occurs in the wall-normal and spanwise mean-squared velocity fluctuations over nearly the entire domain height ($y^+ > 5$), as shown in Fig. 2(c) and (d), especially around the peak (14% and 16% lower in the wall-normal and spanwise directions compared between $case1_S$ and $case1_L$ at $y^+ \approx 40$). With increasing domain size from $case1_S$ to $case1_M$, we find all fluid one-point statistics of $case1_M$ agreeing very well with $case1_L$, demonstrating that the medium domain size ($L_x = 6h$ and $L_z = 3h$) is sufficiently large for reproducing identical fluid one-point statistics as those in the larger domains in the open channel flow configuration. This is similar to the observation of Lozano-Durán and Jiménez (2014) in the wall-bounded channel flow cofiguration.

4. One-point statistics of particle-laden flow

In unladen flow, the domain size of $case1_L$ is demonstrated to be sufficiently large to reproduce identical fluid one-point statistics as those in the larger domains. In Fig. 3, we furthermore compare the particle one-point statistics of $cases4_{L,M,S}$ with the very large domain size simulation of $cases4_{DL}$. The mean velocity and mean-squared velocity fluctuations in three directions can be found in Fig. 3(a–d), respectively. The particle one-point statistics of $case4_L$ are identical with those of $case4_{DL}$, demonstrating that the large domain size is sufficiently large for reproducing identical particle one-point statistics as those in the larger domains in the open channel flow configuration.

In the work of Wang and Richter (2019b), they demonstrate that the range of Stokes number from $St^+ = 2.42$ to $St^+ = 908$ is sufficiently wide to capture two distinct, non-monotonic particle accumulation behaviours in the inner and outer layers. Concentration of moderate Stokes number ($St^+ = 24.2 - 60.5$) particles shows a peak in the inner layer whereas the concentration of low and high Stokes number ($St^+ = 2.42$ and $St^+ = 908$) particles shows a peak in the outer layer. However, with very low particle inertia ($St^+ = 2.42$), particles distribute more homogeneously than moderate particle inertia ($St^+ = 24.2$) in the inner layer, whereas with very high particle inertia ($St^+ = 908$), particles behave ballistically in the outer flow region, again tending to distribute more homogeneously. In this section, we show the domain size effect on particle one-point statistics between the large, medium and small domain sizes for a wide range of Stokes numbers spanning from $St^+ = 2.42$ to $St^+ = 908$. This includes the particle concentration, mean velocity, streamwise flux, mean-squared velocity fluctuations, and particle feedback effect to the carrier phase.

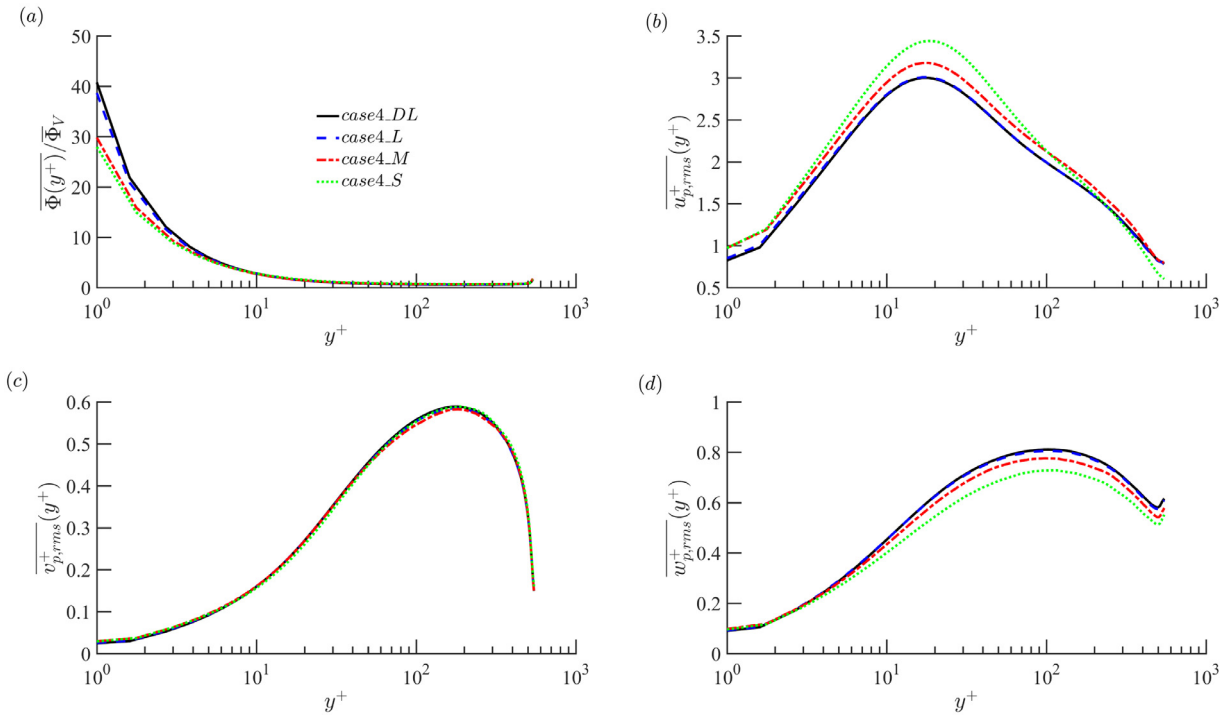

Fig. 3. Comparison of one-point statistics of particles between four different domain sizes (*cases4*$_{DL,L,M,S}$ with $St^+ = 60.5$). (a) Mean particle concentration profiles. (b–d) particle streamwise, wall-normal, and spanwise root mean square velocity fluctuations.

4.1. Particle distribution

The mean particle concentration $\overline{\Phi}$ as a function of the wall-normal direction is shown in Fig. 4(b–f) for increasing Stokes numbers. Vertically-averaged values in three different wall-normal ranges ($y^+ < 10$, $10 < y^+ < 100$ and $100 < y^+ < 500$) are shown in Fig. 4(a). The near-wall particle concentration has a non-monotonic relationship with particle Stokes number, which is low for small ($St^+ = 2.42$ of *case*2 in Fig. 4(b)) and large ($St^+ = 908$ of *case*6 in Fig. 4(f)) Stokes numbers and is high for moderate Stokes numbers ($St^+ = 24.2$ and 60.5 of *case*3 and *case*4 in Fig. 4(c) and (d), respectively). The effect of domain size on mean particle concentration can be clearly observed in Fig. 4(a), where both the small and medium domain sizes underpredict (around 21.7%) the near-wall particle accumulation ($y^+ < 10$), especially for moderate Stokes number particles ($St^+ = 24.2$ and 60.5). However, the domain size only has minimal effect on the particle concentration in the LSMs ($10 < y^+ < 100$) and VLSMs ($100 < y^+ < 500$). Currently, there are two plausible explanations for underprediction of particle concentration close to the wall: one is due to the insufficient domain dimensions which induces an artificial correlation in the velocity field and leads to blocking effects of the particle aggregation (Sardina et al., 2012), or the other which is the missing of particle transport by VLSMs in the small domain simulation (Wang and Richter, 2019a).

From a quadrant analysis, the so-called Q_2 and Q_4 motions are related to ejection and sweep events and the Q_1 and Q_3 motions are called outward and inward interactions (Wallace, 2016). Inertial particles are transferred toward the wall by sweeps and ejected away from the wall by ejections, where they accumulate in the low-speed streaks (Marchioli and Soldati, 2002; Sardina et al., 2012; Zhao et al., 2013; Wang and Richter, 2019b). Particle numbers in the four quadrants can be counted by testing the sign correlation of u'_f and v'_f, where u'_f and v'_f are the fluid fluctuation velocities seen by the particle. This particle number ratio in four quadrants is defined as $R_p^{Q_i} = N_p^{Q_i}/N_p$ ($i = 1-4$) where $N_p = \sum_{i=1}^{4} N_p^{Qi}$ is the particle number in the horizontal slab and $N_p^{Q_i}$ is the particle number in different quadrants. This ratio, cast in terms of the effective volume concentration corresponding to these particle counts, is shown in Fig. 5(a) for *case*3$_{L,M,S}$. It is clear that the particle number in the ejections (Q_2) is dominant in the inner layer whereas the particle number in the sweeps (Q_4) is dominant in the outer layer. Furthermore, particle numbers in 'upwelling' and 'downwelling' regions can be counted by testing whether $u'_f < 0 (Q_2 + Q_3)$ or $u'_f > 0 (Q_1 + Q_4)$, which is shown in Fig. 5(b). Similar to previous findings, there are more particles in the upwelling events than in the downwelling events in the inner layer, which is opposite compared to the outer layer. In the small domain simulation, the particle number ratio in the upwelling events is almost unchanged close to the wall ($y^+ < 10$), underpredicted in the inner layer ($10 < y^+ < 100$), and overpredicted in the outer layer ($y^+ > 100$). This is again opposite compared to the downwelling events. With increasing domain size, the particle number ratio in the ejections and sweeps are nearly the same between the medium size simulation and large size simulation.

4.2. Particle mean velocity

The effect of domain size on mean particle velocity ($\overline{u_p}^+$) is shown in Fig. 6(b–f) as a function of the wall-normal direction for the five Stokes numbers. With increasing Stokes number, the mean particle velocity gradually approaches a logarithmic relationship over nearly the entire domain, particularly for *case*6 at very high Stokes number ($St^+ = 908$). In single-phase flow (Fig. 2(a)), the $\overline{u}$ discrepancy between different domain sizes appears in the outer region ($y^+ > 200$). This discrepancy still exists for moderate and high Stokes number particles, i.e. *cases*3 – 5 as shown in Fig. 6(b–e), respectively. However, the domain size effect disappears in *case*2 (Fig. 6(b)) and *case*6 (Fig. 6(f)), representing low and

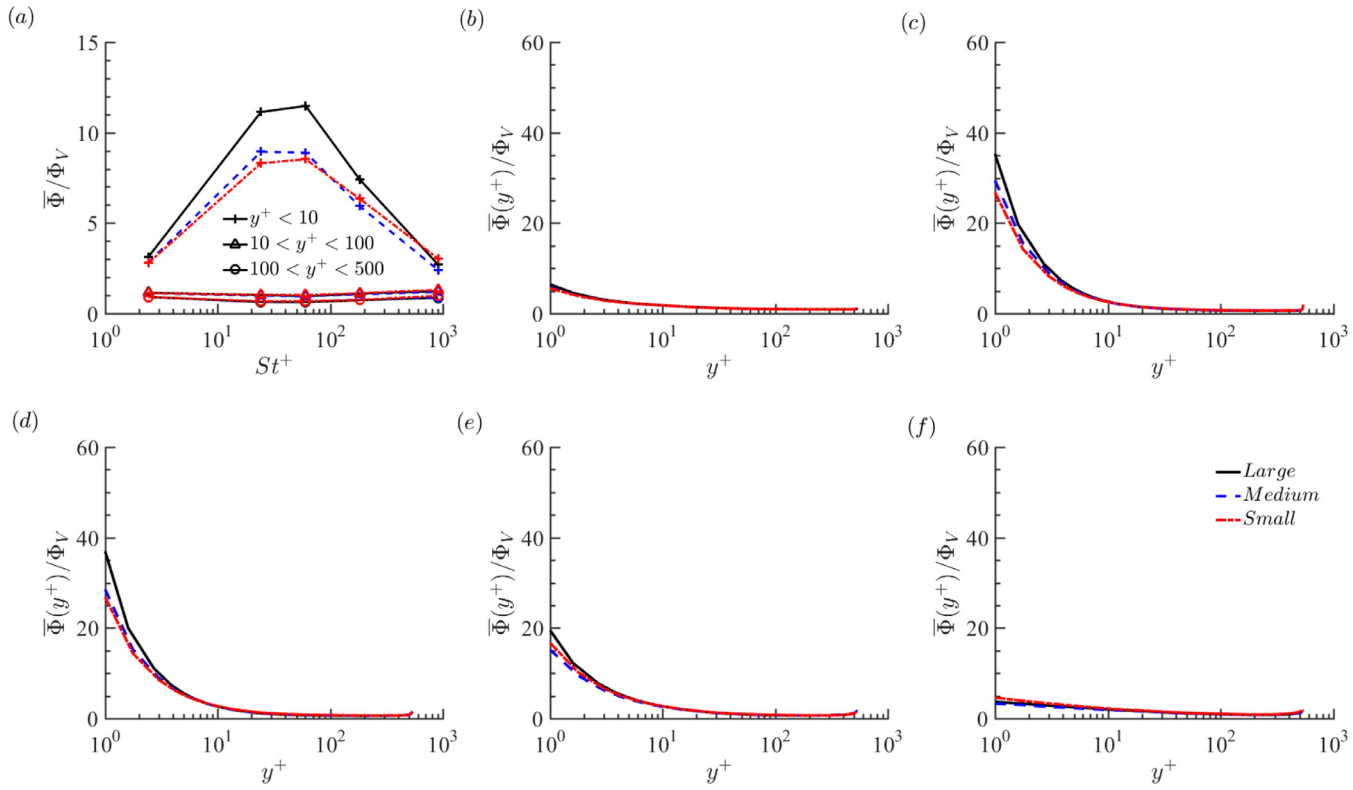

Fig. 4. Domain size effect on mean particle concentration profiles normalized by the bulk concentration. (b–f) *Case*$2-5$ with increasing Stokes numbers $St^+ = 2.42, 24.2, 60.5, 182, 908$, respectively. (a) Average value in the wall-normal direction in three different ranges of height ($y^+ < 10$, $10 < y^+ < 100$ and $100 < y^+ < 500$) as a function of the Stokes number.

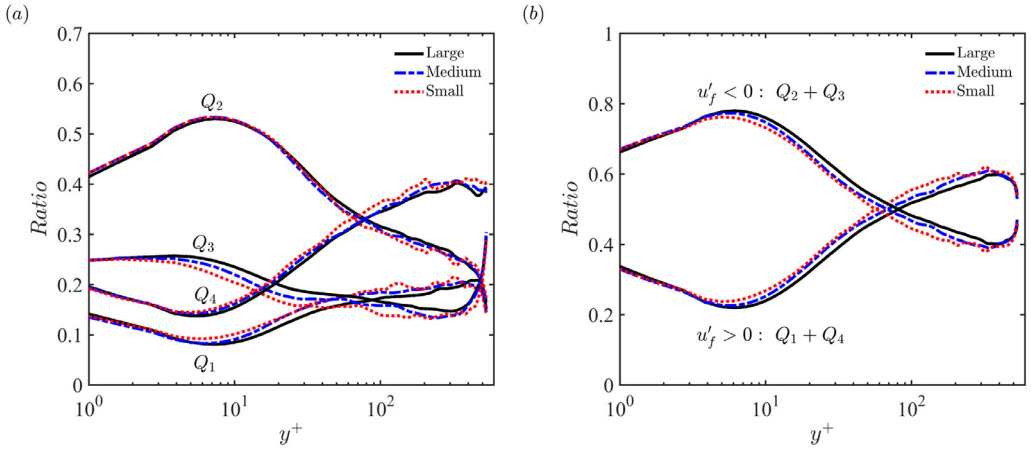

Fig. 5. Particle number ratio in different events compared with total number in wall-normal direction of *case*$3_{L,M,S}$. (a) Particle number ratio $R_p^{Q_i}$ $(i = 1-4)$ of four quadrants; (b) Particle number ratio $R_p^{Q_1+Q_4}$ of $u'_f > 0$ and $R_p^{Q_2+Q_3}$ of $u'_f < 0$.

high Stokes number particles. In the near-wall region ($y^+ < 10$), the domain size effect is negligible for low to high Stokes numbers (*cases*$2-5$). Meanwhile, the domain size difference on the vertically averaged $\overline{u}$ as a function of Stokes number is compared in Fig. 6(a). The three ranges $y^+ < 10$, $10 < y^+ < 100$, and $100 < y^+ < 500$ represent respectively the regions where particles accumulate close to the wall, within the LSMs, and within the VLSMs. The biggest difference in mean particle velocity between the small domain size and the other two larger domain sizes occurs for moderate Stokes number particles ($St^+ = 24.2$) in the range of $100 < y^+ < 500$, which is around 4%.

4.3. Streamwise particle flux

Turbulent particle mass flux, including both the horizontal and wall-normal flux, is an important quantity to be modeled in particle-laden flow. With gravity applied in the wall-normal direction, Richter and Chamecki (2017) examined the role of particle inertia on the particle vertical deposition flux, and whether the resulting concentration profiles follow traditional Rouse theory (Rouse, 1936). Particle inertia is found to deviate from inertialess behaviour, in ways which prove difficult to capture by modifications to the inertialess theory. Particle inertia is also found to

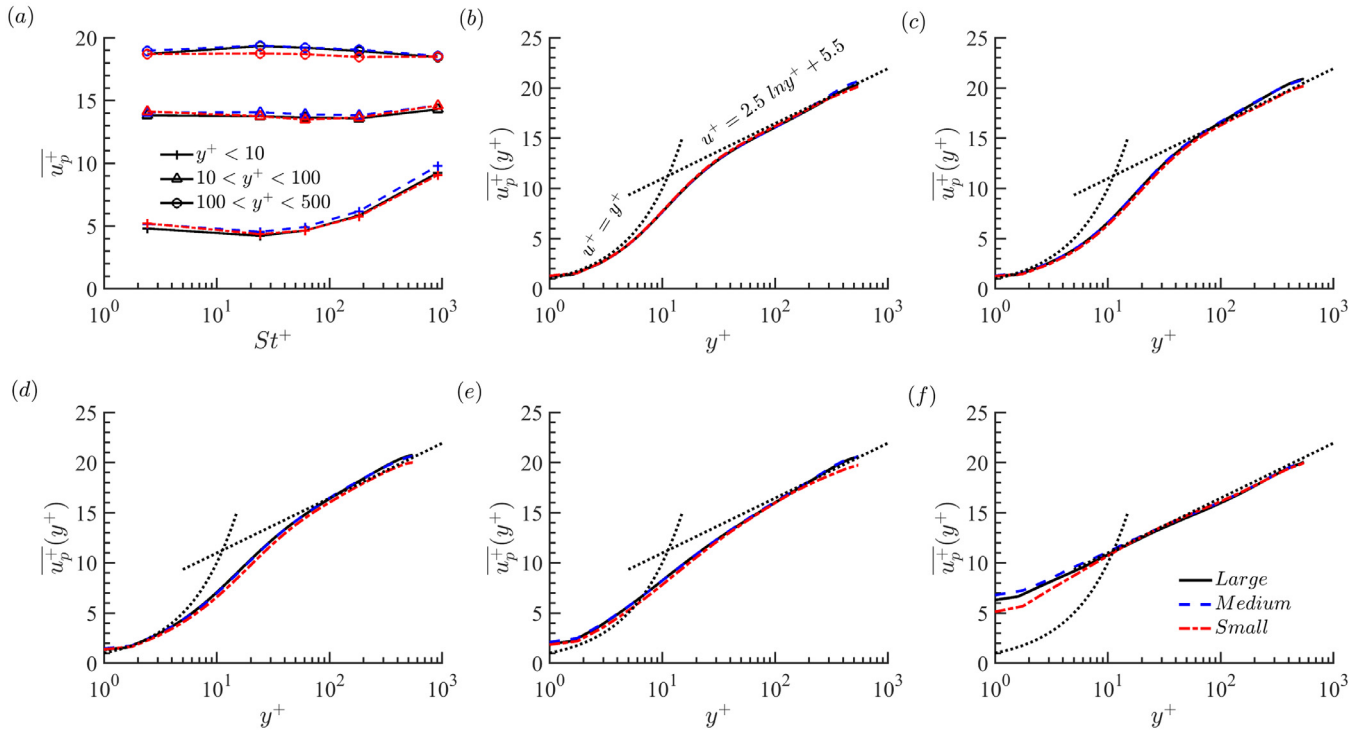

Fig. 6. Domain size effect on mean particle velocity profiles normalized by the viscous velocity scale. (b–f) *Case*$2-5$ with increasing Stokes numbers $St^+ = 2.42, 24.2, 60.5, 182, 908$, respectively. (a) Average value in wall-normal direction for three different ranges of height ($y^+ < 10$, $10 < y^+ < 100$ and $100 < y^+ < 500$) as a function of the Stokes number.

change the relationship between the particle horizontal transport flux and vertical deposition flux (Goossens, 2008). In the present study, we will show the particle streamwise flux from both the Lagrangian and Eulerian point of view.

The mean particle horizontal transport flux $\overline{J_L}$ in the Lagrangian view is defined as mean particle concentration ($\overline{\Phi}$ in Fig. 4) multiplied by the mean particle velocity ($\overline{u_p}$ in Fig. 6) in the horizontal plane, normalized by the bulk values (Φ_V and U_{bulk}, where U_{bulk} is the bulk fluid velocity of the channel), similar to the definition of Noorani et al. (2015). Gravity is not included so that the net particle vertical deposition flux is zero. The domain size effect on the particle horizontal transport flux can be found in Fig. 7. The mean particle horizontal transport flux is shown in Fig. 7(b–f) as a function of wall-normal height for increasing Stokes numbers. In addition, averaged values in wall-normal regions ($y^+ < 10$, $10 < y^+ < 100$ and $100 < y^+ < 500$) are shown in Fig. 7(a) as a function of Stokes number. We see that the domain size has an observable effect only on the particle horizontal mass flux near the wall, especially for moderate Stokes numbers ($St^+ = 24.2$ and 60.5 of *case*3 and *case*4 in Fig. 7(c) and (d), respectively). Both the small and medium domain sizes underpredict (around 20%) the near-wall particle horizontal transport flux ($y^+ < 10$), whereas $\overline{J_L}$ in the LSMs ($10 < y^+ < 100$) and VLSMs ($100 < y^+ < 500$) is hardly affected by the domain size for all Stokes numbers.

From the above discussions regarding domain size effect on the mean particle horizontal transport flux, both the small and medium domain sizes underpredict (around 20%) the near-wall $\overline{J_L}$ for moderate Stokes numbers ($St^+ = 24.2$ and 60.5), which is generally due to the underprediction of the near-wall particle accumulation (Fig. 4) but not the mean particle velocity (Fig. 6).

However, the relationship between particle transport and different turbulent structures is still poorly understood. To explore this coupling between Lagrangian particles with the Eulerian fluid field, we introduce a mean particle horizontal transport flux ($\overline{J_E}$) from an Eulerian point of view, which is defined as the particle concentration on the computational mesh, multiplied by the corresponding fluid streamwise velocity, but filtered according to the wavelengths associated with the small scale and large scale turbulent structures:

$$\begin{aligned} &\textit{Small scale}: \quad J_E = \left|\Phi u_f(\lambda_x^+ < 1375, \lambda_z^+ < 825)\right| \\ &\textit{Large scale}: \quad J_E = \left|\Phi u_f(\lambda_x^+ > 1375, \lambda_z^+ > 825)\right| \end{aligned} \tag{6}$$

Here, the fluid velocity u_f is transferred to Fourier space $\hat{u_f}$, then targeted turbulent structures are filtered (e.g. removing wavelengths with $\lambda_x^+ > 1375, \lambda_z^+ > 825$ to isolate small scale turbulent structures) in order to obtain a filtered fluid velocity field contributed by specific turbulent structures. The filtered $\hat{u_f}$ in Fourier space is inverse transferred to the filtered fluid velocity field (e.g. $u_f(\lambda_x^+ < 1375, \lambda_z^+ < 825)$).

This Eulerian particle streamwise flux $\overline{J_E}$ transported in small scale and large scale turbulent structures for *cases*$3_{L,M,S}$ is shown in Fig. 8(a) and (b), normalized by Φ_{bulk} and u_τ. In the inner layer, the domain size effect results in significant differences for both small scale and large scale $\overline{J_E}$, especially close to the wall ($y^+ < 40$). In addition, both small scale and large scale $\overline{J_E}$ increase with increasing domain size. This indicates that the underprediction of the near-wall particle horizontal transport flux (Fig. 7) by the small domain simulation compared with large domain simulation is due to both the underprediction of the small scale transport (Fig. 8(a)) and missing large scale transport (Fig. 8(b)), which corresponds to the two explanations of particle accumulation shown in Fig. 4 from Sardina et al. (2012) and Wang and Richter (2019a). In the outer layer, the small scale $\overline{J_E}(\lambda_x^+ < 1375, \lambda_z^+ < 825)$ is not sensitive to the domain size (Fig. 8(a)). As discussed above in regards to single-phase flow, the small domain size is too small to capture the VLSMs whereas the medium domain size simulation contains one or two VLSMs. As a consequence, the large scale $\overline{J_E}(\lambda_x^+ > 1375, \lambda_z^+ > 825)$ in the outer layer nearly overlaps between medium domain size and large domain size, which is higher than the small domain size, shown in Fig. 8(b). This means

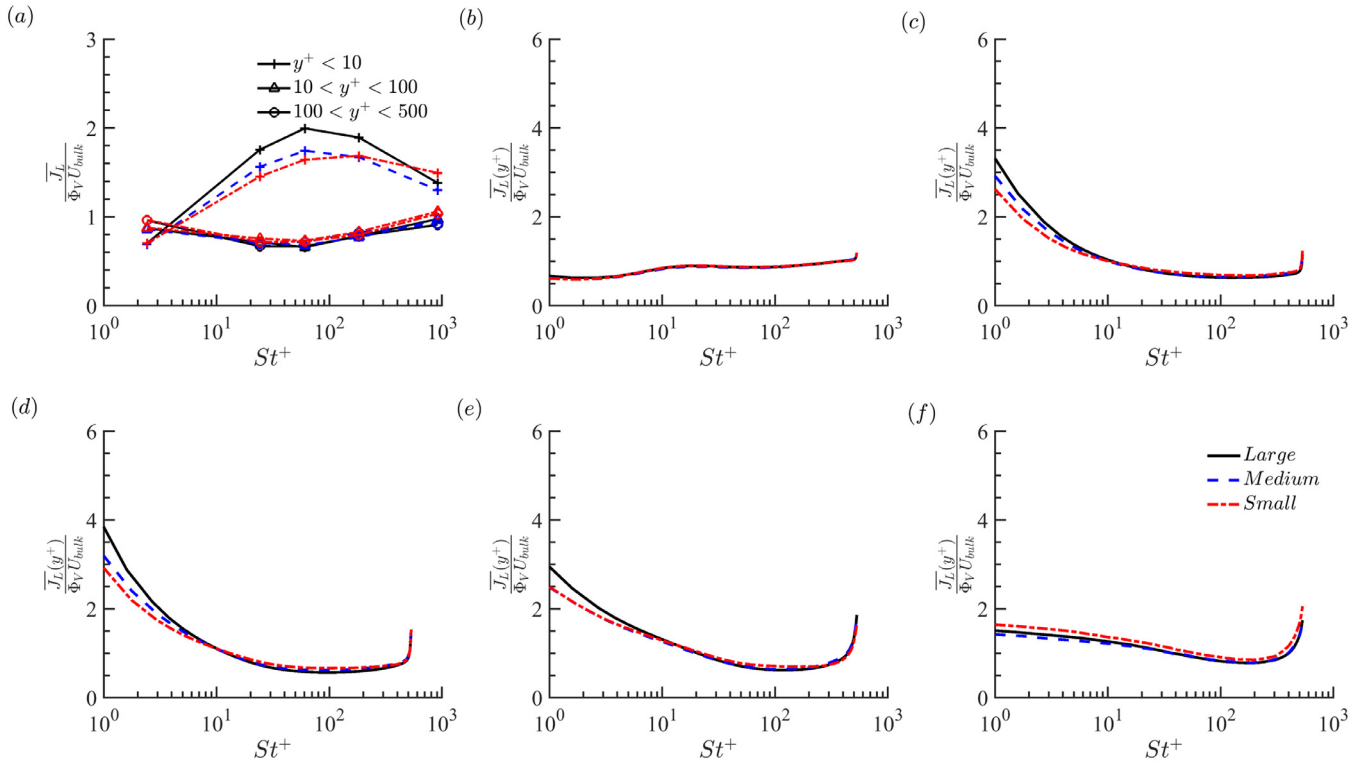

Fig. 7. Domain size effect on the mean streamwise particle fluxes normalized by the bulk velocity and bulk concentration. (b–f) *Case*2 – 5 with increasing Stokes numbers $St^+ = 2.42, 24.2, 60.5, 182, 908$, respectively. (a) Average value in the wall-normal direction, for three different ranges of height ($y^+ < 10$, $10 < y^+ < 100$ and $100 < y^+ < 500$), as a function of the Stokes number.

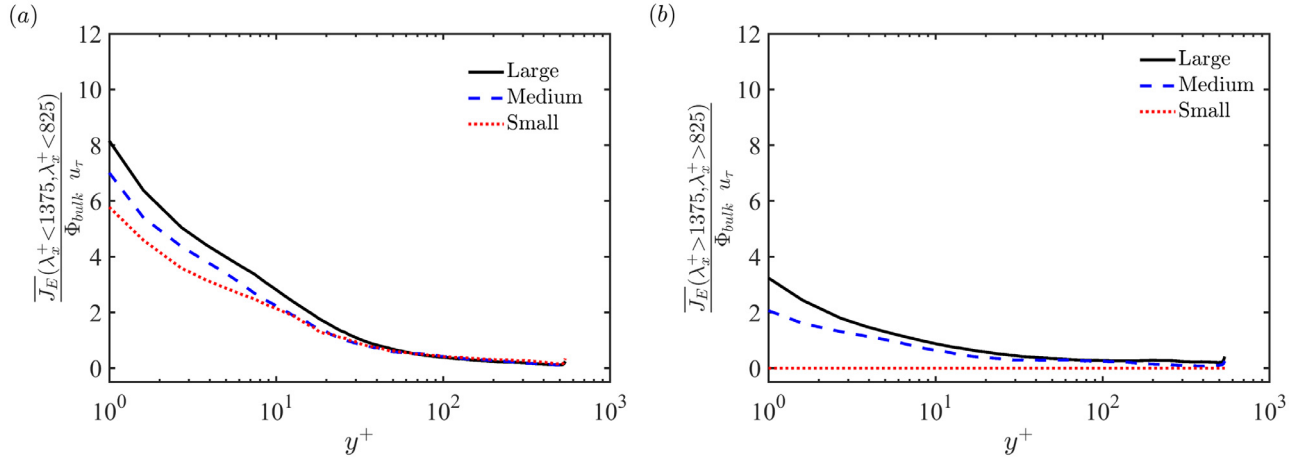

Fig. 8. Domain size effect on the mean streamwise particle fluxes (J_E) normalized by the Φ_{bulk} and u_τ for *case*3$_{L,M,S}$: (a) small scale transport $J_E(\lambda_x^+ < 1375, \lambda_z^+ < 825)$ and (b) large scale transport $J_E(\lambda_x^+ > 1375, \lambda_z^+ > 825)$.

that the medium domain size simulation can reproduce acceptable particle streamwise flux in the outer layer, despite only resolving a low number of large-scale structures.

4.4. Mean-squared particle velocity fluctuations

The particle velocity fluctuation variance in each of the coordinate directions (mean-squared velocity fluctuations) and covariance (particle Reynolds shear stress) are important in assessing the quality of simplified models, e.g. particle-laden LES (Vance et al., 2006) and Eulerian fluid/particle prediction of the dispersed phase (Simonin et al., 1993).

For single-phase flow, as shown in Fig. 2, the maximums of $\overline{u_f'^2}$, $\overline{v_f'^2}$, $\overline{w_f'^2}$ and $-\overline{u_f'v_f'}$ occur at $y^+ = 13.8$, $y^+ = 78.3$, $y^+ = 38.5$, and $y^+ = 44.5$, respectively. Similarly, the profiles of the mean-squared particle velocity fluctuations ($\overline{u_p'^2}^+, \overline{v_p'^2}^+, \overline{w_p'^2}^+$) and Reynolds shear stress ($-\overline{u_p'v_p'}^+$) (figures not shown) first increase and then decrease as a function of y^+, where the maximums occur at $y^+ < 20$ for the streamwise velocity fluctuations and at $50 < y^+ < 200$ for the wall-normal and spanwise velocity fluctuations for the different Stokes numbers. This results in the maximum of the Reynolds shear stress ($-\overline{u_p'v_p'}^+$) occurring at $30 < y^+ < 170$. In Fig. 9(a–d), respectively, we present the wall-normal maximums of the mean-squared velocity fluctuations and Reynolds shear stress. The streamwise velocity fluctuation $\overline{u_p'^2}^+_{max}$ (Fig. 9(a)) only slightly changes as a function of Stokes number in the range $St^+ = 2.42$ to 181, whereas it has a great increase for very high

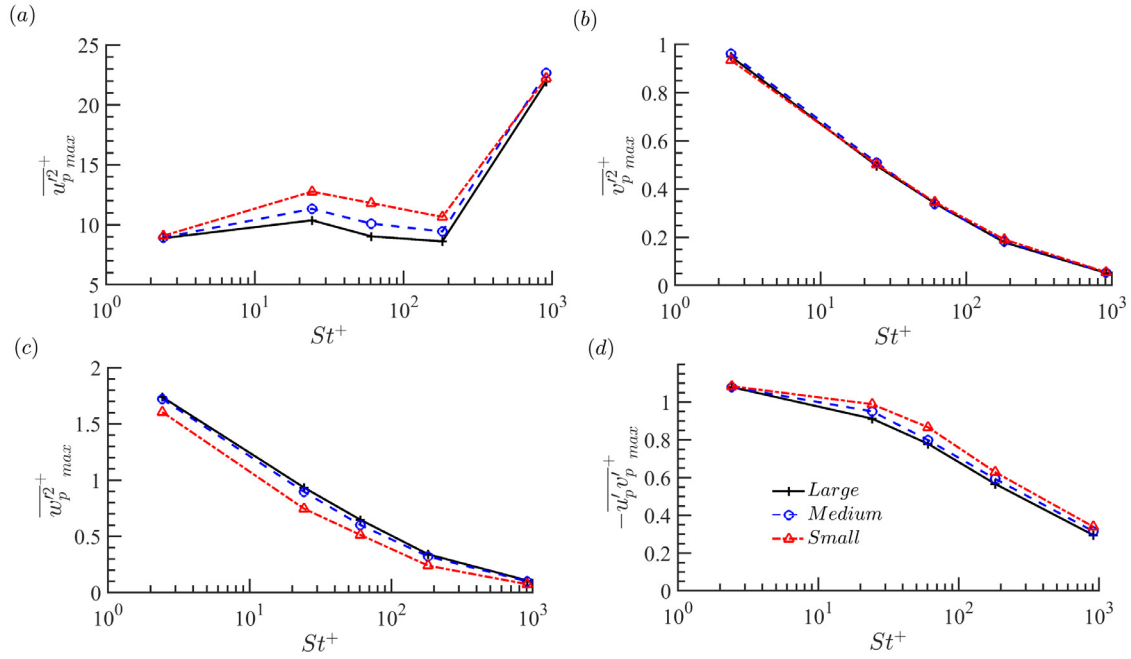

Fig. 9. Domain size effect on the wall-normal maximum of (a-c) the particle mean-squared velocity fluctuations $\overline{u_p'^2}$, $\overline{v_p'^2}$, $\overline{w_p'^2}$, and (d) Reynolds shear stress, as a function of the Stokes number.

Stokes number particles ($St^+ = 908$). In both the wall-normal and spanwise directions, $\overline{v_{p\,max}'^2}^+$ (Fig. 9(b)) and $\overline{w_{p\,max}'^2}^+$ (Fig. 9(c)) decrease nearly linearly with increasing Stokes number (on a logarithmic scale), which is similar to the particle Reynolds shear stress ($-\overline{u_p'v_p'}^+_{max}$) shown in Fig. 9(d). Regarding the domain size effect, the smaller domain sizes (~ 23% for the small domain size and ~ 9% for the medium domain size) overpredict the $\overline{u_{p\,max}'^2}^+$ compared with large domain size at moderate Stokes numbers ($St^+ = 24.2$ and 60.5). On the contrary, $\overline{w_{p\,max}'^2}^+$ is underpredicted ($7 - 12\%$) by the small domain size for all Stokes numbers considered in this study. In the wall-normal direction, $\overline{v_{p\,max}'^2}^+$ is not strongly affected by the domain size. With decreasing domain size, the increased mean-squared streamwise velocity fluctuation and unchanged mean-squared wall-normal velocity fluctuation results in an increase of the Reynolds shear stress (Fig. 9(d)) for moderate Stokes numbers (8% for $St^+ = 24.2$ and 11% for $St^+ = 60.5$). Comparing Fig. 9(a–c) with the corresponding quantities in the unladen flow shown in Fig. 2(b–d), the domain size has a different effect on the particles compared with what happens to the unladen fluid velocity fluctuations. This is largely due to the particle number ratio in the four quadrants (Fig. 5(a)) being different between the small and large domains.

To further explore the relationship between the particle concentration in the upwelling and downwelling events and the streamwise velocity fluctuation and the Reynolds shear stress, the joint PDF of particle concentration with the fluid streamwise fluctuation velocity and Reynolds shear stress in the horizontal planes $y^+ = 20$ and $y^+ = 37$ are plotted in Fig. 10(a) and (b). These heights, i.e. $y^+ = 20$ and $y^+ = 37$, correspond to the wall-normal location of $\overline{u_{p\,max}'^2}^+$ and $-\overline{u_p'v_p'}^+_{max}$ for *case*3, respectively. The particle volume fraction is projected onto the Eulerian grid of the fluid field, allowing for particle concentration to be coupled with the fluid field to retrieve the joint PDF. Fig. 10(a) shows that the difference between large, medium and small domain mainly comes from $u_f' < 0$. This indicates that higher particle concentration (Φ) correlates with greater negative streamwise velocity fluctuations (u_f'), corresponding to more particles accumulating in stronger upwelling events in the small domain compared to those in the medium and large domains. As a consequence, we find that high particle concentration (Φ) correlates with high Reynolds shear stress ($-\overline{u_f'v_f'}$) in the small domain, as shown in Fig. 10(b). Currently, it is commonly accepted that the ejection (Q_2) and sweep (Q_4) events are dominant in contributing the Reynolds shear stress (Wallace, 2016). Based on Fig. 10(a) and (b), we believe that higher particle concentrations occur in the stronger ejection regions in small domain than what is seen in the large domain.

4.5. Interphasial interaction

For particles with high inertia, a significant slip velocity can exist, which describes the exchange of momentum between the fluid and particle phases. A good prediction of the slip velocity is essential to predicting particle trajectories in particle-laden LES (Fede and Simonin, 2006), Reynolds-averaged Navier-Stokes (RANS) coupled laden with Lagrangian particles (Arcen and Tanière, 2009), or two-fluid modeling approaches (Simonin et al., 1993). Through the slip velocity, the drag force governs the particle trajectories and segregation (Marchioli and Soldati, 2002), and subsequently modulates the turbulent flow (Tanaka and Eaton, 2008; Zhao et al., 2013; Wang and Richter, 2019b). Recently, (Wang and Richter, 2019a) found that the particle feedback force to the carrier phase is mainly determined by particle coupling with LSMs (as opposed to VLSMs) in both the inner and outer layers.

As shown in Figs. 1 and 2 in Section 3, only one or two LSMs are captured by the small domain size simulation, while the correct one-point statistics can be reproduced in the near-wall region; i.e. $\overline{u}$ at $y^+ < 100$, $\overline{u'^2}$ at $y^+ < 100$, $\overline{v'^2}$ at $y^+ < 30$ and $\overline{w'^2}$ at $y^+ < 10$. Regarding the particle feedback force in the streamwise (Fig. 11(a)) and wall-normal direction (Fig. 11(b)), the domain size has a minor effect on the particle feedback force which indicates that the particle feedback force is generally due to particle coupling with LSMs, consistent with Wang and Richter (2019a). Furthermore, particle source to the turbulent kinetic energy (TKE) transport equation, defined as $\overline{F_x'u' + F_y'v' + F_z'w'}$, is shown in Fig. 11(c). The particle modulation of the turbulent

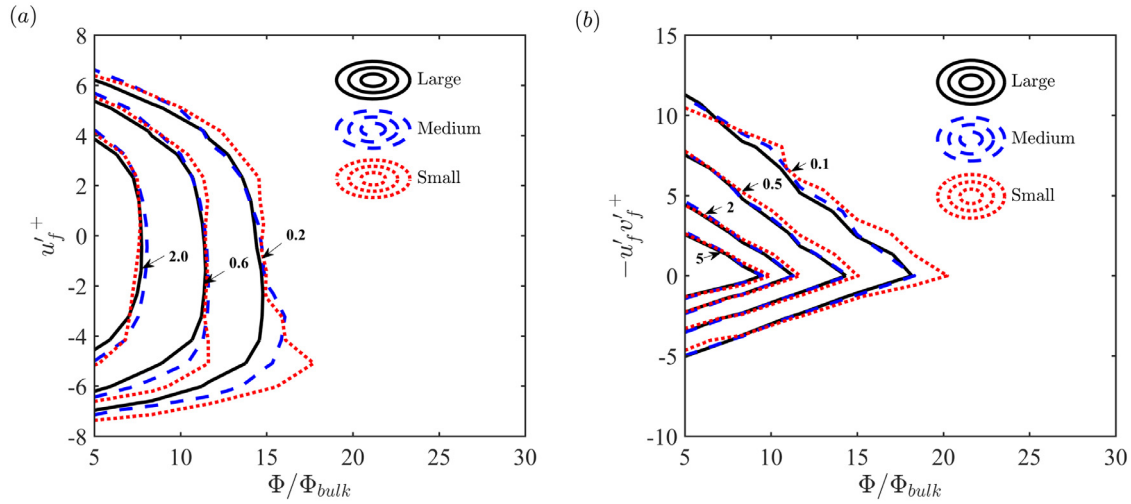

Fig. 10. Domain size effect on the joint PDF of particle concentration with (a) streamwise fluid velocity fluctuation (u_f') in the horizontal plane at $y^+ = 20$; (b) the Reynolds shear stress ($-u'v'$) in the horizontal plane at $y^+ = 37$, for $case3_{L,M,S}$.

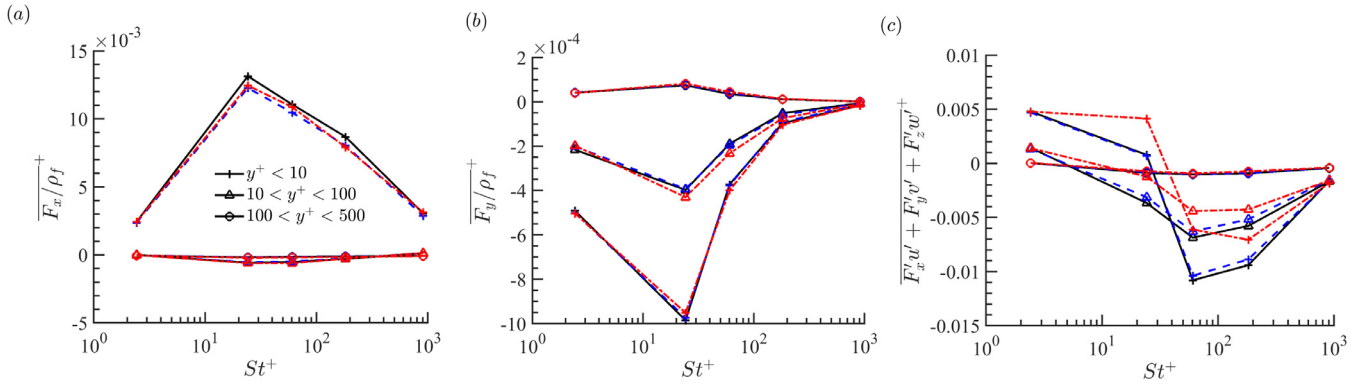

Fig. 11. Average value of (a, b) the streamwise and wall-normal particle feedback force; (c) particle source to the TKE transport equation, in three different ranges of height ($y^+ < 10$, $10 < y^+ < 100$ and $100 < y^+ < 500$) as a function of the Stokes number.

structures (LSMs and VLSMs) is both directly and indirectly related to the particle source term (Wang and Richter, 2019b). Even though the contribution of the particle force is nearly unchanged by the small domain size, its effect to the TKE transport equation has a high sensitivity to domain size, especially in the inner layer ($y^+ < 100$) for moderate and high Stokes numbers ($24.2 \leq St^+ \leq 181$). On the other hand, the medium domain size is large enough to reproduce both the particle feedback force and particle source term to the TKE transport equation. This indicates that in order to reproduce the correct particle source term, it is necessary that the particle feedback force works on the correct turbulent structures. Even though the particle force can be reproduced by the small domain size, the turbulent structures are not fully and accurately captured by the small domain size, which results in the incorrect particle source term to the TKE transport equation.

4.6. Tests at Reynolds number Re_τ=950

For wall turbulence, Re_τ is a ratio of the inner and outer length scales (Marusic et al., 2010). In the outer layer, particles experience turbulent forcing with a characteristic time scale $\tau_{VLSM} \sim h/max(v'|w')$ of VLSMs, where $max(v'|w') \sim u_\tau$ at $y^+ \sim 60$ in this paper. In the inner layer, the characteristic time scale of LSMs is $\tau_{LSM} \sim \delta_\nu/u_\tau$. The ratio of particle Stokes number based on the outer layer turbulence time scale (VLSMs) and the inner layer turbulence time scale (LSMs) can be seen as $St^{outer}/St^+ \equiv (\tau_p/\tau_{VLSM})/(\tau_p/\tau_{LSM}) = \tau_{LSM}/\tau_{VLSM} \sim \delta_\nu/h$. Clearly, the ratio of particle Stokes number between the outer layer and inner layer is proportional to $1/Re_\tau$ where the friction Reynolds number is defined by $Re_\tau \equiv h/\delta_\nu$. Comparing between particle-laden flows at low and high Reynolds numbers, the same St^+ based on the inner time scale corresponds to lower St^{outer} based on the outer time scale at the higher Reynolds number.

At a low Reynolds number $Re_\tau = 180$, a significant increasing of wall particle accumulation (up to 20%) is found in the large domain in comparison with small domain, which is due to intensive turbophoresis at $St^+ = 10 - 50$ when the particle time scale matches the time scale of LSMs in the inner layer (Sardina et al., 2012). In this paper, we find similar behavior at an intermediate Reynolds number of $Re_\tau = 550$; i.e., the particle accumulation is underpredicted by the small domain simulation, especially for moderate Stokes numbers ($St^+ = 24.2$ and 60.5). Furthermore, we perform tests of the domain size effect on particle statistics for two Stokes numbers ($St^+ = 39.8$ and 182) at an even higher Reynolds number of $Re_\tau = 950$. The mean particle concentration profiles for $St^+ = 39.8$ and 182 are shown in Fig. 12 (a) and (b), respectively. Similar to $Re_\tau = 180$ and 550, the particle wall concentration is observed to be largest in the large domain simulation compared to the medium and small domain sizes for both of the tested Stokes numbers, especially at $St^+ = 39.8$. Clearly for $Re_\tau = 180$, 550 and 950, the domain size effect on particle accumulation in the vicinity

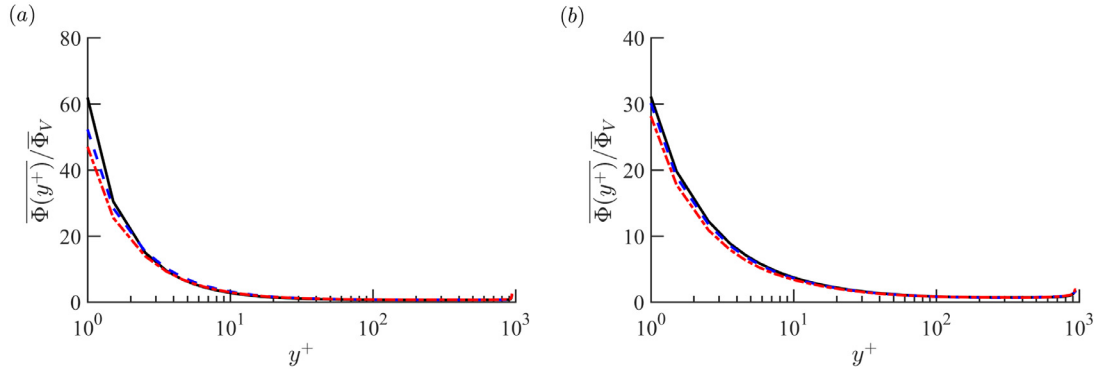

Fig. 12. Domain size effect of (a) case7 and (b) case8 at $Re_\tau = 950$, on the mean particle concentration profile normalized by the bulk concentration.

of the wall is closely related to $St^+ \sim O(10)$ based on the viscous scale but not St^{outer} based on the outer time scale. We speculate that this behavior can still be observed in the limit of constant St^+ but increasing Re_τ to a higher value.

5. Conclusion

In this brief study, inertial particle one-point statistics are presented for direct numerical simulations of turbulent open channel flow at a moderate Reynolds number ($Re_\tau = 550$), which are seeded with two-way coupled particles at low volume concentration for a wide range of particle Stokes numbers ($2.41 \leq St^+ \leq 908$). The domain size effect on the particle one-point statistics is examined for three different domain dimensions, i.e. a large domain $L_x = 6\pi h, L_z = 2\pi h$, medium domain $L_x = 6h, L_z = 3h$, and small domain $L_x = 2.5h, L_z = 1.5h$, where h is the depth of the open channel.

In single-phase open channel flow, we find that the medium domain size ($L_x = 6h, L_z = 3h$) simulation can reproduce the fluid one-point statistics produced in a large domain (larger than $L_x = 6\pi h, L_z = 2\pi h$), which also agrees very well with an extreme domain size ($L_x = 60\pi h, L_z = 6\pi h$) in wall-bounded channel flow (Lozano-Durán and Jiménez, 2014). In the case of particle-laden flow, for low ($St^+ = 2.42$) and very high ($St^+ = 908$) Stokes numbers, all of the particle one-point statistics (mean streamwise particle flux, TKE, particle feedback to the carrier phase) are well-captured by the medium domain size simulation with reference to the large domain size simulation. On the other hand, a discrepancy between the medium domain and the large domains appears for moderate and high Stokes numbers ($24.2 \leq St^+ \leq 182$). Taking the moderate Stokes number $St^+ = 24.2$ as an example, in the near-wall region the mean streamwise particle flux is underpredicted (~ 20%) below $y^+ < 10$, which is mainly due to the underpredicted particle accumulation and not the mean particle streamwise velocity in this region. By analyzing the filtered particle flux transported by small and large scale turbulent structures, we show that the insufficient domain dimensions induce an artificial correlation in the velocity field lead to blocking effects of the particle aggregation, in agreement with Sardina et al. (2012). Apart from the particle accumulation close to the wall, differences are also observed in the maximum of mean-squared steamwise velocity fluctuation (~ 9%) and Reynolds shear stress (~ 8%). The joint PDF of particle concentration with fluid steamwise velocity fluctuation and fluid Reynolds shear stress shows that higher particle concentration is associated with large negative u_f' and positive $-u_f'v_f'$ in smaller domains.

With decreasing domain size, the previously mentioned differences are increased between the small domain and the large domain, especially for moderate Stokes numbers ($St^+ = 24.2$ and 60.5). Regarding to the mean particle feedback forces to the carrier phase, the domain size has a negligible effect for all Stokes numbers, since the particle feedback force to the carrier phase is determined by particle coupling with LSMs in both the inner and outer layer (Wang and Richter, 2019a). However, the particle source to the TKE transport equation has differs considerably between the small and large domain simulations, especially in the inner layer ($y^+ < 100$) for moderate and high Stokes numbers ($24.2 \leq St^+ \leq 181$).

Based on above comparison of domain size effect for low to very high Stokes number particles, particle one-point statistics of low ($St^+ = 2.42$) and very high ($St^+ = 908$) Stokes numbers can be well-reproduced by small domain simulations in both the inner layer and outer layer. For moderate to high ($St^+ = 24.2 - 182$) Stokes numbers, however, the medium domain size cannot reproduce accurate particle one-point statistics in the inner layer compared to those of the large domain, especially close to the wall. This is due to the insufficient resolution of the VLSM effects within the inner layer, which are referred to as deep u-modes (del Alamo and Jiménez, 2013) or VLSM 'footprints' (Hutchins and Marusic, 2007). In the outer layer, although the medium domain only contains one or two VLSMs, particle one-point statistics seem to be well-reproduced by the medium domain size simulation compared with the large domain. This indicates that large domain size is necessary to reproduce accurate particle one-point statistics in the inner layer whereas medium domain size is sufficient to reproduce accurate particle one-point statistics in the outer layer when studying high Reynolds number particle-laden flows.

Declaration of Competing Interest

The authors declare that they have no known competing financial interests or personal relationships that could have appeared to influence the work reported in this paper.

CRediT authorship contribution statement

Guiquan Wang: Conceptualization, Methodology, Formal analysis, Writing - original draft. **Hyungwon John Park:** Formal analysis, Writing - review & editing. **David H. Richter:** Software, Writing - review & editing, Supervision.

Acknowledgments

The authors acknowledge grants G00003613-ArmyW911NF-17-0366 from the US Army Research Office and N00014-16-1-2472 from the Office of Naval Research. Computational resources were

provided by the High Performance Computing Modernization Program (HPCMP), and by the Center for Research Computing (CRC) at the University of Notre Dame.

References

Adrian, R.J., Marusic, I., 2012. Coherent structures in flow over hydraulic engineering surfaces. J. Hydraul. Res. 50 (5), 451–464.

del Alamo, J. C., Jiménez, J., 2013. Direct numerical simulation of the very large anisotropic scales in a turbulent channel. arXiv:1309.2322

Arcen, B., Tanière, A., 2009. Simulation of a particle-laden turbulent channel flow using an improved stochastic lagrangian model. Phys. Fluids 21 (4), 043303.

Capecelatro, J., Desjardins, O., 2013. An euler–lagrange strategy for simulating particle-laden flows. J. Comput. Phys. 238, 1–31.

Capecelatro, J., Desjardins, O., 2015. Mass loading effects on turbulence modulation by particle clustering in dilute and moderately dilute channel flows. J. Fluids Eng. 137 (11), 111102.

Capecelatro, J., Desjardins, O., Fox, R.O., 2018. On the transition between turbulence regimes in particle-laden channel flows. J. Fluid Mech. 845, 499–519.

Del Álamo, J.C., Jiménez, J., 2003. Spectra of the very large anisotropic scales in turbulent channels. Phys. Fluids 15 (6), L41.

Fede, P., Simonin, O., 2006. Numerical study of the subgrid fluid turbulence effects on the statistics of heavy colliding particles. Phys. Fluids 18 (4), 045103.

Flores, O., Jiménez, J., 2010. Hierarchy of minimal flow units in the logarithmic layer. Phys. Fluids 22 (7), 071704.

Fong, K.O., Amili, O., Coletti, F., 2019. Velocity and spatial distribution of inertial particles in a turbulent channel flow. J. Fluid Mech. 872, 367–406.

Goossens, D., 2008. Relationships between horizontal transport flux and vertical deposition flux during dry deposition of atmospheric dust particles. J. Geophys. Res. 113 (F2).

Guala, M., Hommema, S., Adrian, R., 2006. Large-scale and very-large-scale motions in turbulent pipe flow. J. Fluid Mech. 554, 521–542.

Hamilton, J.M., Kim, J., Waleffe, F., 1995. Regeneration mechanisms of near-wall turbulence structures. J. Fluid Mech. 287, 317–348.

Hutchins, N., Marusic, I., 2007. Evidence of very long meandering features in the logarithmic region of turbulent boundary layers. J. Fluid Mech. 579, 1–28.

Hwang, Y., Cossu, C., 2010. Self-sustained process at large scales in turbulent channel flow. Phys. Rev. Lett. 105 (4), 044505.

Jiménez, J., 2011. Cascades in wall-bounded turbulence. Annu. Rev. Fluid. Mech. 44 (1), 27.

Jiménez, J., Moin, P., 1991. The minimal flow unit in near-wall turbulence. J. Fluid Mech. 225, 213–240.

Jiménez, J., Pinelli, A., 1999. The autonomous cycle of near-wall turbulence. J. Fluid Mech. 389, 335–359.

Kidanemariam, A.G., Chan-Braun, C., Doychev, T., Uhlmann, M., 2013. Direct numerical simulation of horizontal open channel flow with finite-size, heavy particles at low solid volume fraction. New J. Phys. 15 (2), 025031.

Kim, K.C., Adrian, R.J., 1999. Very large-scale motion in the outer layer. Phys. Fluids 11 (2), 417–422. doi:10.1063/1.869889.

Kline, S.J., Reynolds, W., Schraub, F., Runstadler, P., 1967. The structure of turbulent boundary layers. J. Fluid Mech. 30 (4), 741–773.

Lee, J., Lee, C., 2019. The effect of wall-normal gravity on particle-laden near-wall turbulence. J. Fluid Mech. 873, 475–507.

Lovecchio, S., Marchioli, C., Soldati, A., 2013. Time persistence of floating-particle clusters in free-surface turbulence. Phys. Rev. E 88 (3), 033003.

Lozano-Durán, A., Jiménez, J., 2014. Effect of the computational domain on direct simulations of turbulent channels up to re $\tau = 4200$. Phys. Fluids 26 (1), 011702.

Marchioli, C., Soldati, A., 2002. Mechanisms for particle transfer and segregation in a turbulent boundary layer. J. Fluid Mech. 468, 283–315.

Marchioli, C., Soldati, A., Kuerten, J., Arcen, B., Taniere, A., Goldensoph, G., Squires, K., Cargnelutti, M., Portela, L., 2008. Statistics of particle dispersion in direct numerical simulations of wall-bounded turbulence: results of an international collaborative benchmark test. Int. J. Multiph. Flow 34 (9), 879–893.

Marusic, I., Mathis, R., Hutchins, N., 2010. Predictive model for wall-bounded turbulent flow. Science 329 (5988), 193–196.

Maxey, M.R., Riley, J.J., 1983. Equation of motion for a small rigid sphere in a nonuniform flow. Phys. Fluids 26 (4), 883–889.

Moser, R.D., Kim, J., Mansour, N.N., 1999. Direct numerical simulation of turbulent channel flow up to re $\tau = 590$. Phys. Fluids 11 (4), 943–945.

Nagaosa, R., Handler, R.A., 2003. Statistical analysis of coherent vortices near a free surface in a fully developed turbulence. Phys. Fluids 15 (2), 375–394.

Nakagawa, H., Nezu, I., 1981. Structure of space-time correlations of bursting phenomena in an open-channel flow. J. Fluid Mech. 104, 1–43.

Narayanan, C., Lakehal, D., Botto, L., Soldati, A., 2003. Mechanisms of particle deposition in a fully developed turbulent open channel flow. Phys. Fluids 15 (3), 763–775.

Noorani, A., Sardina, G., Brandt, L., Schlatter, P., 2015. Particle velocity and acceleration in turbulent bent pipe flows. Flow, Turbulence and Combustion 95 (2-3), 539–559.

Pan, Y., Banerjee, S., 1996. Numerical simulation of particle interactions with wall turbulence. Phys. Fluids 8 (10), 2733–2755.

Pedinotti, S., Mariotti, G., Banerjee, S., 1992. Direct numerical simulation of particle behaviour in the wall region of turbulent flows in horizontal channels. Int. J. Multiph. Flow 18 (6), 927–941.

Richter, D., Chamecki, M., 2017. Inertial effects on the vertical transport of suspended particles in a turbulent boundary layer. Bound.-Layer Meteor. 1–22.

Rouse, H., 1936. Modern Conceptions of the Mechanics of Fluid Turbulence. American Society of Civil Engineers. https://books.google.com/books?id=fWfbtgAACAAJ

Sardina, G., Schlatter, P., Brandt, L., Picano, F., Casciola, C.M., 2012. Wall accumulation and spatial localization in particle-laden wall flows. J. Fluid Mech. 699, 50–78.

Schiller, V., 1933. ber die grundlegenden berechnungen bei der schwerkraftaufbereitung. Z. Vereines Deutscher Inge. 77, 318–321.

Simonin, O., Deutsch, E., Minier, J., 1993. Eulerian prediction of the fluid/particle correlated motion in turbulent two-phase flows. Appl. Sci. Res. 51 (1-2), 275–283.

Tanaka, T., Eaton, J.K., 2008. Classification of turbulence modification by dispersed spheres using a novel dimensionless number. Phys. Rev. Lett. 101 (11), 114502.

Vance, M.W., Squires, K.D., Simonin, O., 2006. Properties of the particle velocity field in gas–solid turbulent channel flow. Phys. Fluids 18 (6), 63302.

Vreman, A., 2015. Turbulence attenuation in particle-laden flow in smooth and rough channels. J. Fluid Mech. 773, 103–136.

Wallace, J.M., 2016. Quadrant analysis in turbulence research: History and evolution. Annu. Rev. Fluid. Mech. 48, 131–158.

Wang, G., Fong, K.O., Coletti, F., Capecelatro, J., Richter, D., 2019. Inertial particle velocity and distribution in vertical turbulent channel flow: a numerical and experimental comparison. Int. J. Multiph. Flow 103105.

Wang, G., Richter, D., 2019a. Transport and two-way coupling effect of inertial particles by large-scale and very-large-scale motions in turbulence. arXiv:1906.01779

Wang, G., Richter, D.H., 2019. Two mechanisms of modulation of very-large-scale motions by inertial particles in open channel flow. J. Fluid Mech. 868, 538559. doi:10.1017/jfm.2019.210.

Yamamoto, Y., Kunugi, T., Serizawa, A., 2001. Turbulence statistics and scalar transport in an open-channel flow. J. Turbul. 2 (10), 1–16.

Zhao, L., Andersson, H.I., Gillissen, J.J., 2013. Interphasial energy transfer and particle dissipation in particle-laden wall turbulence. J. Fluid Mech. 715, 32.